



HAL
open science

A systematic ab initio study of vacancy formation energy, diffusivity, and ionic conductivity of $\text{Ln}_2\text{NiO}_{4+\delta}$ (Ln=La, Nd, Pr)

Songge Yang, Guangchen Liu, Yueh-Lin Lee, Jean-Marc. Bassat, Jacinthe Gamon, Antoine Villesuzanne, John Pietras, Xiao-Dong Zhou, Yu Zhong

► To cite this version:

Songge Yang, Guangchen Liu, Yueh-Lin Lee, Jean-Marc. Bassat, Jacinthe Gamon, et al.. A systematic ab initio study of vacancy formation energy, diffusivity, and ionic conductivity of $\text{Ln}_2\text{NiO}_{4+\delta}$ (Ln=La, Nd, Pr). *Journal of Power Sources*, 2023, 576, pp.233200. 10.1016/j.jpowsour.2023.233200. hal-04112388

HAL Id: hal-04112388

<https://hal.science/hal-04112388>

Submitted on 31 May 2023

HAL is a multi-disciplinary open access archive for the deposit and dissemination of scientific research documents, whether they are published or not. The documents may come from teaching and research institutions in France or abroad, or from public or private research centers.

L'archive ouverte pluridisciplinaire **HAL**, est destinée au dépôt et à la diffusion de documents scientifiques de niveau recherche, publiés ou non, émanant des établissements d'enseignement et de recherche français ou étrangers, des laboratoires publics ou privés.

A Systematic Ab Initio Study of Vacancy Formation Energy, Diffusivity and Ionic Conductivity of $\text{Ln}_2\text{NiO}_{4+\delta}$ (Ln=La, Nd, Pr)

Songge Yang¹, Guangchen Liu¹, Yueh-Lin Lee^{2,3}, Jean-Marc Bassat⁴, Jacinthe Gamon⁴, Antoine Villesuzanne⁴, John Pietras⁵, Xiao-Dong Zhou⁶, Yu Zhong¹

¹*Mechanical and Materials Engineering, Worcester Polytechnic Institute, 100 Institute Rd, Worcester, MA, 01609, USA*

²*National Energy Technology Laboratory, 626 Cochran Mill Road, Pittsburgh, PA 15236, USA*

³*NETL Support Contractor, 626 Cochran Mill Road, Pittsburgh, PA 15236, USA*

⁴*CNRS, Univ. Bordeaux, ICMCB, 87 Av. Dr. Schweitzer, 33608 Pessac, France*

⁵*Saint-Gobain Research North America, Northborough, MA 01532, USA*

⁶*Institute for Materials Research and Innovation, Department of Chemical Engineering, University of Louisiana at Lafayette, Lafayette, Louisiana 70503, USA*

Abstract

This study systematically investigates the vacancy formation energy, diffusivity, and ionic conductivity of the $\text{Ln}_2\text{NiO}_{4+\delta}$ (Ln=La, Nd, Pr, and $\delta=0.125$) compound using the ab initio approach. Specifically, the impact of thermal expansion on the oxygen transport properties is considered, using a combination of quasi-harmonic approximation (QHA) and a linear regression model to study and reproduce the temperature-dependent properties of $\text{Ln}_2\text{NiO}_{4+\delta}$. Overall, the predictions are in excellent agreement with previous theoretical studies in the literature. It is confirmed that the ionic transport properties of the $\text{Ln}_2\text{NiO}_{4+\delta}$ are not dominated by oxygen vacancy diffusion due to the high vacancy formation energy. Additionally, the interstitialcy

mechanism, which involves interstitial O²⁻ hopping parallel to the a-b plane with the rocksalt layer, is determined to be the more favorable diffusion path. Meanwhile, the predicted energy barrier, diffusion coefficient, and ionic conductivity of Ln₂NiO_{4+δ} show reasonable agreement with experimental data, with Pr₂NiO_{4+δ} exhibiting the lowest activation energy barrier ($\Delta E_b=0.722$ eV) and the highest thermal expansion, diffusivity, and ionic conductivity. Overall, this study presents an efficient and computationally facile tool for predicting ionic transport properties in materials where thermal expansion is the main driving force for temperature-dependent properties.

Keywords: *ab initio*, diffusivity, ionic conductivity, r-SOCs, activation energy barrier

1. Introduction

In the past decade, the $Ln_2NiO_{4+\delta}$ ($Ln=La, Nd, Pr$) Ruddlesden-Popper (RP) family with the K_2NiF_4 -type structure has attracted a lot of attention. $Ln_2NiO_{4+\delta}$ has been proposed as a performant air electrode material in reversible solid oxide cells (r-SOCs), which is capable of working in both solid oxide fuel cell (SOFC) mode and solid oxide electrolyzer cells (SOECs) mode [1-6]. Compared with the traditional air electrode materials, the $Ln_2NiO_{4+\delta}$ RP phase has a higher resistance to Cr-poisoning under SOFC operating conditions, which prevents performance degradation [7]. Additionally, the $Ln_2NiO_{4+\delta}$ structure has excellent oxygen transport properties [8-19]. These structures consist of sheets of NiO_6 octahedral sharing corners interleaved by Ln_2O_2 layers where the additional oxygen is localized [9, 20]. Furthermore, it has been demonstrated that the interstitialcy mechanism with the oxygen occupying the interstitial layers is the main contributor to oxygen ion transport [21, 22].

So far, extensive experimental studies have been conducted on the oxygen transport properties of the $Ln_2NiO_{4+\delta}$ compounds and their doped counterpart. Bassat et al.[23] measured the oxygen diffusion coefficient for single crystals of both $Pr_2NiO_{4+\delta}$ and $Nd_2NiO_{4+\delta}$ along the two main crystallographic orientations. They found the oxygen diffusion along the a - b plane for $Pr_2NiO_{4+\delta}$ is higher than that of $Nd_2NiO_{4+\delta}$ due to a much lower diffusion activation energy. Boehm et al. investigated the oxygen diffusion and transport properties in non-stoichiometric $Ln_{2-x}NiO_{4+\delta}$ ($Ln=La, Nd, Pr$) oxides [9]. They concluded that the oxygen diffusion performance of $Pr_2NiO_{4+\delta}$ is the highest among the studied compounds. Regarding the doped $Ln_2NiO_{4+\delta}$ compounds, Shen et al. observed that the ionic conductivity of $La_2NiO_{4+\delta}$ compounds increases significantly with the increasing Ca-doping level (up to $x=0.1$ of $La_{2-x}Ca_xNiO_{4+\delta}$) on the La site [24]. Meanwhile, Hyodo

et al. concluded that the doping of Cu and Ga enhanced the oxygen diffusion properties of the $\text{Pr}_2\text{NiO}_{4+\delta}$ [8].

The oxygen transport properties of the $\text{Ln}_2\text{NiO}_{4+\delta}$ compounds have been the object of various theoretical studies; see references [25-37] for examples. The interstitialcy diffusion mechanism was revealed by both atomistic [25, 26] and first-principles molecular dynamics [27], and the role of the apical oxygen atoms and lattice dynamics (low-energy-phonons) in this mechanism was assessed from first-principles [27, 31, 34]. The effects of strain and oxygen overstoichiometry were investigated by molecular dynamics [25, 26] and DFT [28, 29, 36]. Additionally, Xu et al. [28] and Sadykov et al. [37] discussed the possible existence of peroxide ions as intermediate species in the diffusion process with the DFT simulations. Defect energetics and their influence on diffusion were investigated by classical molecular dynamics [30] and DFT [29, 35].

Accordingly, the aim of the present work is to systematically investigate the vacancy formation energy, diffusivity, and ionic conductivity of the $\text{Ln}_2\text{NiO}_{4+\delta}$ ($\delta = 0.125$) compounds through the *ab initio* approach by coupling 0 K DFT volume-dependent properties with the quasi-harmonic approximation which gives the temperature-dependent free energy as a function of volume. The nudged elastic band (NEB) method is adopted to predict the energy barrier, diffusion coefficient, and ionic conductivity of the oxygen ions. In order to accurately describe the strong correlation effects of the transition metal Ni, and f-orbital Pr and Nd, the a rotationally invariant GGA+U approach was used to improve the accuracy of the calculations. Furthermore, considering the change of the oxygen transport properties caused by the thermal expansion effect, a combination of the quasi-harmonic approximation (QHA) and a linear regression model is used to study and reproduce the temperature-dependent properties of the $\text{Ln}_2\text{NiO}_{4+\delta}$ RP phases. According

to QHA, the physical properties such as energy barrier [38], elasticity [39], and magnetism [40] can be estimated as a function of temperature and volume when the thermal expansion is taken into account. This method enables predicting temperature-dependent properties solely caused by thermal expansion without using more fastidious molecular dynamic simulations. Finally, the comparison between the *ab initio* modeling and available experimental data from the literature is also discussed.

2. Methodology

2.1 *Ab initio* computational details

The *ab initio* calculations were applied using the Vienna *ab initio* simulation package (VASP) [41, 42]. Throughout the study, the generalized gradient approximation (GGA) [43] with the Perdew-Burke-Ernzerhof (PBE) exchange-correlation function [44] has been utilized using the projector augmented wave method. The k-point meshes with a density of no less than 5000 (per-reciprocal atom) were used to sample the Brillouin zones. The accurate total energy calculations were applied using the linear tetrahedron method with Blöchl's corrections [45]. The total energies obtained by relaxation calculations were converged to 10^{-6} eV/cell with a 1.75 times plane-wave cutoff energy suggested by the corresponding element pseudopotentials. Meanwhile, the static calculations, which converged to 10^{-8} eV/cell with 520 eV cutoff energy, were applied after each relaxation procedure. Finally, the calculated static energies were fitted by the Birch-Murnaghan equation of state [46] for each structure to get a more accurate total energy. For the magnetic order, both ferromagnetic (FM) and antiferromagnetic (AFM) were considered for the Ni atoms (**See S1 in the supplementary file**). The present work adopted the structure with the most stable magnetic configuration.

Although the *ab initio* calculations provide good agreement with the experiments for metallic systems as well as a reasonable trend for the geometry and reactivity of metal oxides and molecular systems, this method fails to obtain the correct electronic structure for the strongly correlated system due to errors associated with on-site Coulomb and exchange interactions [47, 48]. These errors limit the applicability of the *ab initio* calculations in late-transition metal oxides and rare-earth compounds [49]. A possible workaround is using the GGA+*U* method, which considers local corrections within selected orbitals. The value of *U* is chosen to match experimentally observed properties or computational results performed with a high level of theory [15]. It has been reported that a reasonably broad range for the Ni cations was selected between 4.5-8.5 eV. Accordingly, in the present study, we only adopt the value of *U*=6 eV for Ni, based on previous studies in the literature [15, 50]. The optimal *U* value for Pr *f*-orbitals is selected to be 3 eV according to the recent study proposed by Staykov et al. [15].

Meanwhile, the optimization of the *U* value for Nd *f*-orbitals has been performed. The results were fitted to the electronic density of states (EDOS) (**See S2 in the supplementary file**) obtained with the Heyd–Scuseria–Ernzerhof (HSE06) hybrid function. From Figure S2, it is concluded that the EDOS obtained with PBE function using GGA+*U* with *U*=6 eV for both Ni *3d*- and Nd *4f*-orbitals reproduces the EDOS and band gap obtained with the HSE06 functional near the fermi energy. Thus, the optimal *U* value for Nd *f*-orbitals is selected as 6 eV in the present work.

The oxygen stoichiometric $Ln_2NiO_{4.0}$ ($Ln=La, Nd, Pr$) compounds were selected for the present work's total energy, vacancy formation energy, and thermal expansion coefficient calculations. The lattice parameters and space group of $La_2NiO_{4.0}$, $Nd_2NiO_{4.0}$, and $Pr_2NiO_{4.0}$ are included in the supplementary file (**See S3 in the supplementary file**), containing the comparison

between the experimental and ab initio value (See Table S1 and S2 in the supplementary file). The Phonon frequency calculations are carried out by the supercell method, implemented in *YPHON* code [51], from force constants calculated with VASP. The present work used 126-atom supercells for the calculations of Ln_2NiO_4 and 228-atom supercells for the calculations of $Ln_2NiO_{4+\delta}$. In the VASP calculations, a $4 \times 4 \times 4$ k-point mesh for the 126-atom supercell and a $3 \times 3 \times 3$ k-point mesh for 228-atom supercells were used, respectively. The forces induced by small displacements were calculated.

Finally, the activation barrier was obtained based on the climbing NEB (CI-NEB) method implemented in the VTST code [52]. In this section, the diffusion properties of the over-stoichiometric $Ln_2NiO_{4+\delta}$ with $\delta=0.125$ was estimated, i.e., the NEB simulations were performed with the formula: $Ln_{16}Ni_8O_{33}$. Considering the computational expense, only one image between the starting and ending geometries was applied, in which the NEB force converged to 0.05 eV \AA^{-2} . Throughout this study, the graphical visualization package VESTA [53] was used to check the ionic positions in each NEB image.

2.2 Quasi-harmonic approximations (QHA)

The free energy of $Ln_2NiO_{4.0}$ can be estimated by QHA as [40, 54-57]:

$$F(V, T) = E(V) + F_{vib}(V, T) + F_{ele}(V, T) \quad (1)$$

where $E(V)$ is the total energy of Ln_2NiO_4 at 0K. It can be calculated and fitted by the Murnaghan equation of states (EOSs) [46]:

$$E(V) = a + \frac{B_0 V}{B'_0} \left(1 + \frac{\left(\frac{V_0}{V}\right)^{B'_0}}{B'_0 - 1} \right) \quad (2)$$

In Eq. (2), the fitting parameter a can be expressed as $E_0 - \frac{B_0 V_0}{B'_0 - 1}$. The parameters V_0 , E_0 , B_0 , and B'_0 represent the equilibrium volume, energy, bulk modulus, and its first derivation with respect to pressure, respectively.

$F_{vib}(V, T)$ and $F_{ele}(V, T)$ are the free energy of Ln_2NiO_4 contributed by phonon and electron, respectively, which can be estimated by:

$$F_{vib}(V, T) = k_B T \int_0^\infty \ln \left[2 \sinh \left(\frac{\hbar \omega}{2k_B T} \right) \right] g(\omega, V) d\omega \quad (3)$$

$$F_{ele}(V, T) = \int n(\varepsilon, V) f \varepsilon d\varepsilon - \int^{\varepsilon_F} n(\varepsilon, V) \varepsilon d\varepsilon + k_B T \int n(\varepsilon, V) [f \ln f + (1 - f) \ln(1 - f)] d\varepsilon \quad (4)$$

where ω represents the phonon frequency, $g(\omega, V)$ represents the PDOS at frequency ω volume V (See S4 in the supplementary file), k_B is Boltzmann's constant, and \hbar is the reduced Planck constant. $n(\varepsilon, V)$ is the electronic density of state (EDOS) with f being the Fermi distribution.

The equilibrium volume $V_{eq}(P, T)$ at given T and P can be obtained by finding the root of the following equation:

$$-\left(\frac{\partial F(V, T)}{\partial V} \right)_T = P \quad (5)$$

3. Result and discussions

3.1 Vacancy formation energy in Ln_2NiO_4 compound

The oxygen point defects are essential for the oxygen reduction reaction (ORR) as they are likely strongly coupled to oxygen dissociation transport and incorporation [47]. In this section, the bulk oxygen vacancy formation energy is investigated to examine the possibility of oxygen

transport in bulk stoichiometric Ln_2NiO_4 compound ($Ln=La, Nd, Pr$). The vacancy formation energy is given by:

$$\Delta E_{Vf} = E_{Ln_2NiO_{4-\delta}}^{ab\ initio}(vac) - E_{Ln_2NiO_4}^{ab\ initio} + \frac{1}{2}(E_{O_2}^{ab\ initio} + \Delta h_{O_2}^0) \quad (6)$$

where $E_{Ln_2NiO_{4-\delta}}^{ab\ initio}(vac)$ and $E_{Ln_2NiO_4}^{ab\ initio}$ are the energies of stoichiometric Ln_2NiO_4 with and without an oxygen vacancy, respectively. $E_{O_2}^{ab\ initio}$ is the *ab initio* calculated energy of the O_2 molecule and $\Delta h_{O_2}^0$ is a correction term, which accounts for errors that do not cancel between the treatment of oxygen in the gas and solid phases. It has been reported that the Perdew-Burke-Ernzerhof (PBE) (O) pseudopotential has an O_2 energy correction $\Delta h_{O_2}^0 = 1.36eV$ [47]. Accordingly, this value is selected as a correction term.

Table 1 Oxygen vacancy (apical /equatorial) formation energy for stoichiometric bulk $Ln_2NiO_{4.0}$ compounds

Vacancy formation Energy (eV/vac)	$La_2NiO_{4-\delta}$	$Nd_2NiO_{4-\delta}$	$Pr_2NiO_{4-\delta}$
Apical site	6.33	6.09	6.15
Equatorial site	5.19	5.03	5.07

The *ab initio* calculated vacancy formation energies of $La_2NiO_{4.0}$, $Nd_2NiO_{4.0}$, and $Pr_2NiO_{4.0}$ are shown in *Table 1*. According to the space group symmetry, there are two non-equivalent oxygen sites in the Ln_2NiO_4 compound: 1) the apical site and 2) the equatorial site. The vacancy formation energy of the apical site is around 1 eV higher than the equatorial site. However, even with the equatorial site, the formation energy of vacancy is about 5.03-5.19 eV/vac. It is very high compared with the barrier of the interstitialcy diffusion mechanism, which holds in the range of

0.5 eV-1.5 eV [25, 26]. Accordingly, the oxygen vacancy diffusion does not play a critical role for the oxygen stoichiometric La_2NiO_4 , Nd_2NiO_4 , and Pr_2NiO_4 compounds.

3.2 The energy barrier calculation of oxygen interstitial in $\text{Ln}_2\text{NiO}_{4+\delta}$

3.2.1. The interstitialcy diffusion mechanism in $\text{Ln}_2\text{NiO}_{4+\delta}$

It has been reported that the stoichiometric tetragonal Ln_2NiO_4 phases have several O^{2-} interstitialcy migration pathways along the a - b plane and the c -axis [58]. As the oxygen partial pressure increases, the O^{2-} will occupy the interstitial site in the Ln_2O_2 layers and form $\text{Ln}_2\text{NiO}_{4+\delta}$. It was reported that Ln_2NiO_4 could incorporate additional oxygen up to $\delta=0.18$ for La_2NiO_4 [22, 29, 59, 60] and $\delta=0.22$ for Nd_2NiO_4 and Pr_2NiO_4 [37, 61], respectively, and even to larger values if thermal treatments under oxygen pressure are applied [36].

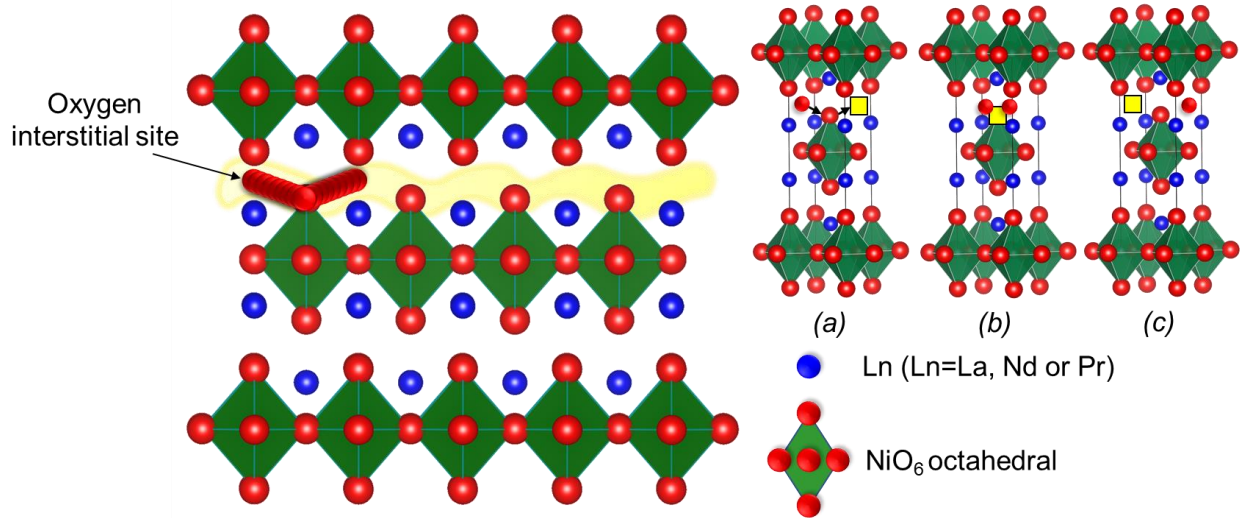


Figure 1 The diffusion mechanism of O^{2-} in $\text{Ln}_2\text{NiO}_{4+\delta}$

The diffusion mechanism of $\text{Ln}_2\text{NiO}_{4+\delta}$ is shown in Figure 1. In the initial configuration, as shown in the unit cell (a) of Figure 1, the O^{2-} intercalates in the Ln_2O_2 layer, resulting in over-stoichiometric phases $\text{Ln}_2\text{NiO}_{4+\delta}$. Meanwhile, the apical O^{2-} from one of these octahedra is able to move upwards towards an unoccupied interstitial site with the corresponding relaxation. In the

intermediate state (Figure 1 unit cell (b)), the apical O^{2-} takes up the residence in an adjacent interstitial site, and the vacancy is formed at the apical site. Meanwhile, the initial interstitial O^{2-} is ready to move toward the apical site of the NiO_6 octahedron. Finally, the original interstitial O^{2-} reforms at the NiO_6 octahedron again, as shown in the unit cell (c) of Figure 1. The procedure will repeat in the next unit cell, and the oxygen ion can move along with the path marked in yellow, as shown in the left figure.

To determine if other pathways for the oxygen diffusion of the $Ln_2NiO_{4+\delta}$ compound can be considered, the present study employed the *ab initio* simulation to investigate three possible migration pathways and to evaluate the migration energy barriers. The schematic diagram of these three pathways is shown in Figure 2.

Figure 2 (a) exhibits path #1 of the interstitialcy oxygen migration along with the *a-b* plane, which has been reported by several groups [15, 25, 58] and is already shown in Figure 1. In particular, the interstitial O^{2-} (yellow) will displace an apical O^{2-} (purple) from the NiO_6 octahedron, which moves to an adjacent oxygen interstitial site. Figure 2 (b) shows path #2 of the interstitial oxygen migration along with the *a-b* plane, reported by Frayret et al. [29]. Specifically, this pathway corresponds to direct atomic jumps of the interstitial oxygen between vacant adjacent interstitial sites within the $La_2O_{2.25}$ layer. While path #1 and path #2 both migrate along the *a-b* plane, path #3 was considered to determine the O^{2-} transport along the *c-axis* orientation perpendicular to the *a-b* plane (Figure 2 (c)). In this path, the interstitial O^{2-} (yellow) will move down and displace an apical O^{2-} (purple) from the NiO_6 octahedron, and then the original apical O^{2-} will move down to an adjacent interstitial site.

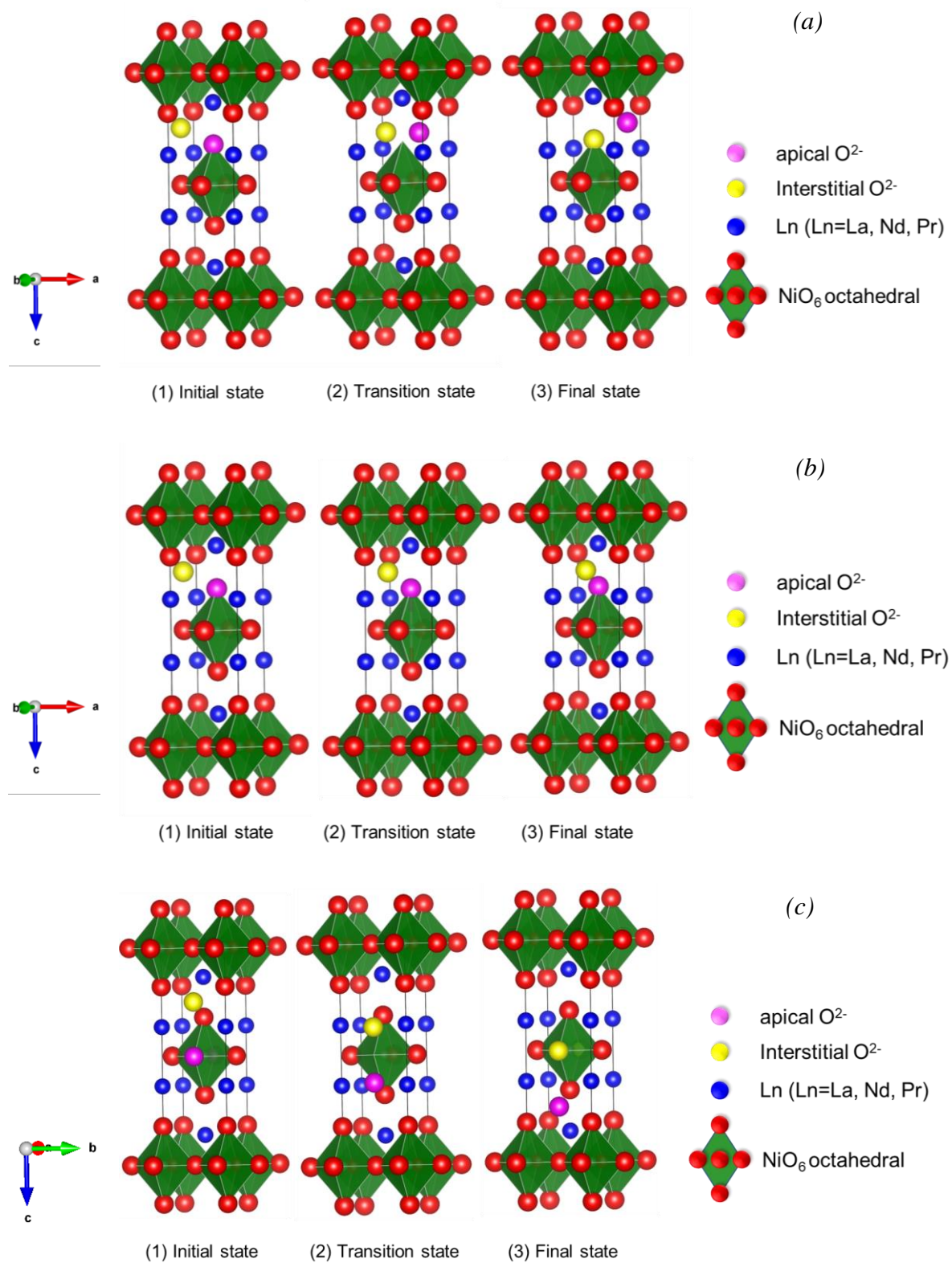


Figure 2 The diffusion paths of O^{2-} in $Ln_2NiO_{4+\delta}$ selected in the present study (a) Path #1 (along with the a-b plane) (b) Path #2 (along with the a-b plane) (c) Path #3 (along with the c-axis).

3.2.2. The energy barrier of different O^{2-} migration paths in the $Ln_2NiO_{4+\delta}$ compound

The energy barriers were estimated by the energy difference between the local minimum point and the saddle point (located around the middle of the migration pathways) of the energy profiles. The results of the predicted energy barriers of the $Ln_2NiO_{4+\delta}$ along different migration paths are shown in Figure 3. Overall, the results show that the energy barriers of path #1 along the a - b plane are energetically favorable for $Ln_2NiO_{4+\delta}$ ($Ln=La, Nd, Pr$) compared to the other pathways. It was also found that the energy barriers for path #2 and path #3 are around 2~3 times higher than the barriers of path #1, which indicates that these two pathways are less likely. Meanwhile, it has been reported [30] that the oxygen diffusion of $La_2NiO_{4+\delta}$ is highly anisotropic, with activation energies such as $E_a(\parallel a, b)=0.3-0.9$ eV and $E_a(\parallel c)=2.9-3.5$ eV. Therefore, it is suggested that the O^{2-} should migrate parallel to the a - b plane (path #1) instead of the c direction.

Based on the energy barriers of path #1 among these three compounds, it is shown that the activation barriers computed are 0.789 eV for $La_2NiO_{4+\delta}$, 0.932 eV for $Nd_2NiO_{4+\delta}$, and 0.722 eV for $Pr_2NiO_{4+\delta}$, respectively. Furthermore, it indicates that the O^{2-} migration along path #1 in $Pr_2NiO_{4+\delta}$ and $La_2NiO_{4+\delta}$ is much easier than in $Nd_2NiO_{4+\delta}$.

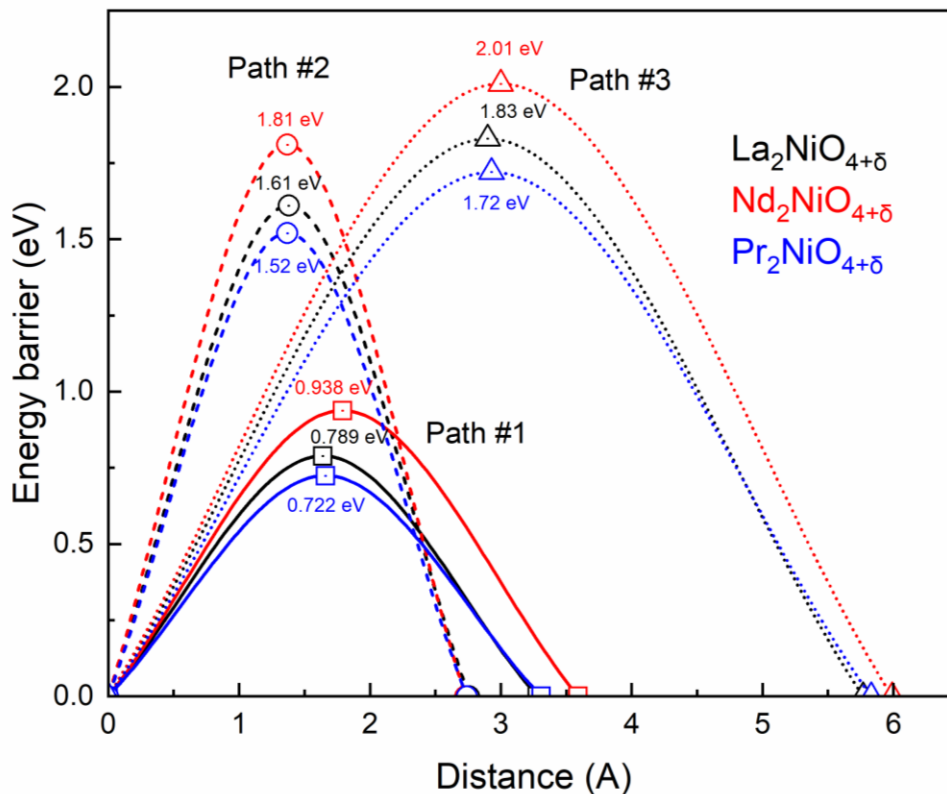


Figure 3 The energy barriers of different O^{2-} migration paths in $Ln_2NiO_{4+\delta}$ (Path #1: solid lines with open square marks; Path #2: short dashed lines with open circle marks; Path #3: short dot lines with open triangle marks; Black color: $La_2NiO_{4+\delta}$; Red color: $Nd_2NiO_{4+\delta}$; Blue color: $Pr_2NiO_{4+\delta}$)

To directly visualize how each ion moves, the ionic positions of $Ln_2NiO_{4+\delta}$ in each NEB image are envisioned through the VESTA package, as shown in Figure 4. The ions unrelated to the NEB procedures (i.e., Ni) are removed from the picture. The yellow O10 and purple O16 in the diagram represent the interstitial and apical O^{2-} , respectively. The green, orange, and blue ions denote La, Nd, and Pr ions, respectively. All the structures shown in Figure 4 were fully relaxed.

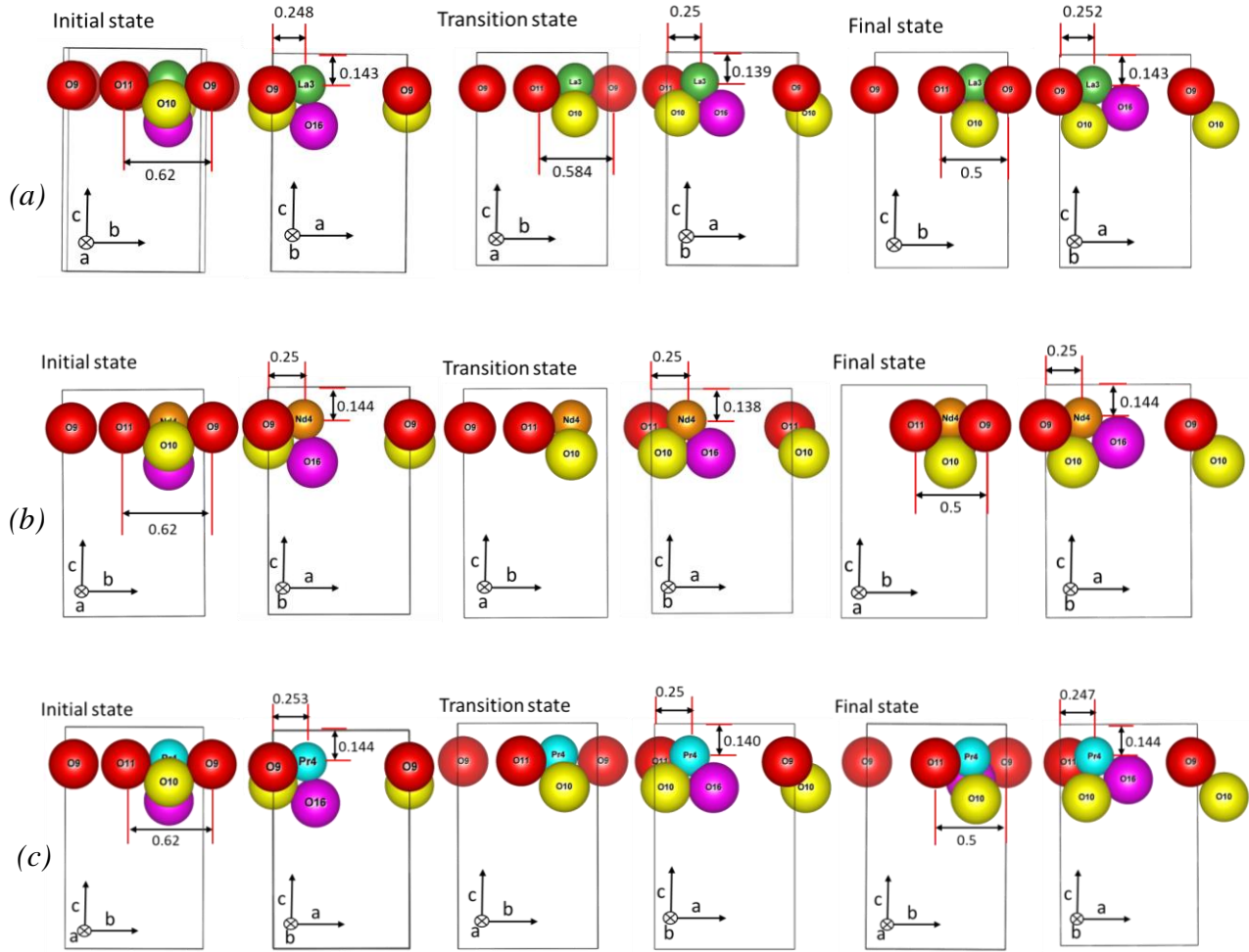


Figure 4 The schematic graph of ionic positions of path #1 at different states, (a) $\text{La}_2\text{NiO}_{4+\delta}$, (b) $\text{Nd}_2\text{NiO}_{4+\delta}$, and (c) $\text{Pr}_2\text{NiO}_{4+\delta}$. (Note: the yellow O10 and purple O16 spheres represent the interstitial and apical oxygen ions, respectively. The green, orange, and blue spheres denote La, Nd, and Pr ions, respectively)

According to the initial state, it is observed that the insertion of O10 will push away O9, O11, and O16, which provides the space for the residence of O10 on the interstitial sites. In this procedure, the distance (fractional coordinate) between O9 and O11 increases from 0.5 to 0.62. During the transition, O10 will move along the a -axis and kick the apical O16 out of the NiO_6 octahedron. Meanwhile, the migration of O10 will push the La, Nd, and Pr ions to overcome

the barrier. At the final stage, O10 reforms at the NiO₆ octahedron, and the original apical O16 will take up the residence at an adjacent interstitial site.

Based on these three NEB images in Figure 4, it could be speculated that the energy barriers of these three compounds at the transition state are closely related to how far La, Nd, and Pr ions travel during the migration of O²⁻. Compared with the original positions of La, Nd, and Pr ions at the initial state, the migration of O10 and O16 will push La, Nd, and Pr ions up 0.004 (from 0.143 up to 0.139), 0.006 (from 0.144 up to 0.138), and 0.004 (from 0.144 up to 0.140) units to overcome the barrier, respectively. It suggests that less activation energy is required to push the La and Pr ions up for 0.004 units than the Nd ion up for 0.006 units, which might be the reason why the barrier of Nd₂NiO_{4+δ} is relatively higher, and the energy barrier of Pr₂NiO_{4+δ} and La₂NiO_{4+δ} are much lower. This result agrees with experimental data from the literature, where the higher activation energy of the neodymium compound was attributed to its smaller *c* lattice parameter [23, 31]. The latter is suggested to be responsible for (i) a shorter inter-octahedral space and (ii) a less pronounced effect of low energy phonon modes, which act as a prerequisite for high oxygen mobility at moderate temperatures.

3.3 The temperature-dependent properties of Ln₂NiO_{4+δ}

In the previous section, the activation energy barriers of different O²⁻ migration paths in Ln₂NiO_{4+δ} compounds for a particular volume were systematically discussed. The volume expansion caused by the temperature increase plays an essential role in determining the temperature-dependent activation energy barrier of Ln₂NiO_{4+δ} and needs to be investigated.

3.3.1. Temperature-dependent equation of states (EOSs) and thermal expansion

The EOSs (based on Eq. (1)) of Ln_2NiO_4 with the change of temperatures were predicted based on the quasi-harmonic approximation (QHA), as shown in Figure S5 (**in the supplementary file**). The black dashed line marks the evolution of the equilibrium volume at $P=0$ atm with increasing temperature. The volume is the cell volume divided by the number of atoms (volume per atom). The temperature-dependent properties were obtained by considering the thermal effect, such as the free energy, crystal volume, and thermal expansion.

The thermal expansion of the La_2NiO_4 , Nd_2NiO_4 , and Pr_2NiO_4 compounds are plotted in Figure 5, including the comparison with experimental data [20, 62, 63] from the literature. It can be calculated based on Eq. (7).

$$\frac{\Delta V}{V_0} = \frac{V_{eq} - V_0}{V_0} \quad (7)$$

where V_{eq} and V_0 represent the temperature-dependent equilibrium volume and equilibrium volume at 0 K, respectively. According to the literature review, Ln_2NiO_4 shows phase transition [64, 65] from tetragonal ($I4/mmm$) to orthorhombic ($Fmmm$) at low temperatures (448K for La_2NiO_4 [64], 823K for Nd_2NiO_4 [64], and 753K for Pr_2NiO_4 , [65] respectively). However, our calculated structure is the high-temperature tetragonal phase. Therefore, to make an apple-to-apple comparison, the reference state temperatures of these three phases are selected as the phase transition temperature. It should be noted that the original experimental data for these three compounds are based on linear thermal expansion. However, the calculated thermal expansions by QHA are based on the volume thermal expansion. Therefore, the present study approximately converted the linear expansion experimental data to the volume expansion experimental data by using Eq (8) [66] to make a direct comparison:

$$\frac{\Delta V}{V_0} = 3 \frac{\Delta L}{L_0} \quad (8)$$

Figure 5 (a) shows that the calculated thermal expansion of La_2NiO_4 is in excellent agreement with the experimental data proposed by Makhnach et al. [62]. In contrast, without the consideration of the U value for f-orbital Nd and Pr, the predicted thermal expansion of Nd_2NiO_4 and Pr_2NiO_4 (the blue line in Figure 5 (b) and Figure 5 (c)) exhibit significant discrepancies with the experimental data [20, 63] with the change of temperature. The maximum differences in volume expansions between *ab initio* and literature data are 0.43% for Nd_2NiO_4 and 0.38% for Pr_2NiO_4 at 300K. After adopting the optimized U parameter for both Nd and Pr, the agreements of thermal expansion between the *ab initio* prediction and experimental data [20, 63] are greatly improved. The slope of the thermal expansion has a reasonable agreement with the experimental data. Based on the experimental data, it was found that the phase transition from tetragonal ($I4/mmm$) to orthorhombic ($Fmmm$) does not have a significant effect on the slope of the thermal expansion in Ln_2NiO_4 . However, the discrepancies at low temperatures might cause by the phase transition. The comparison of thermal expansion in these three compounds is plotted in Figure 5 (d). Based on our simulations, the Pr_2NiO_4 compound exhibits much higher thermal expansion than Nd_2NiO_4 and La_2NiO_4 .

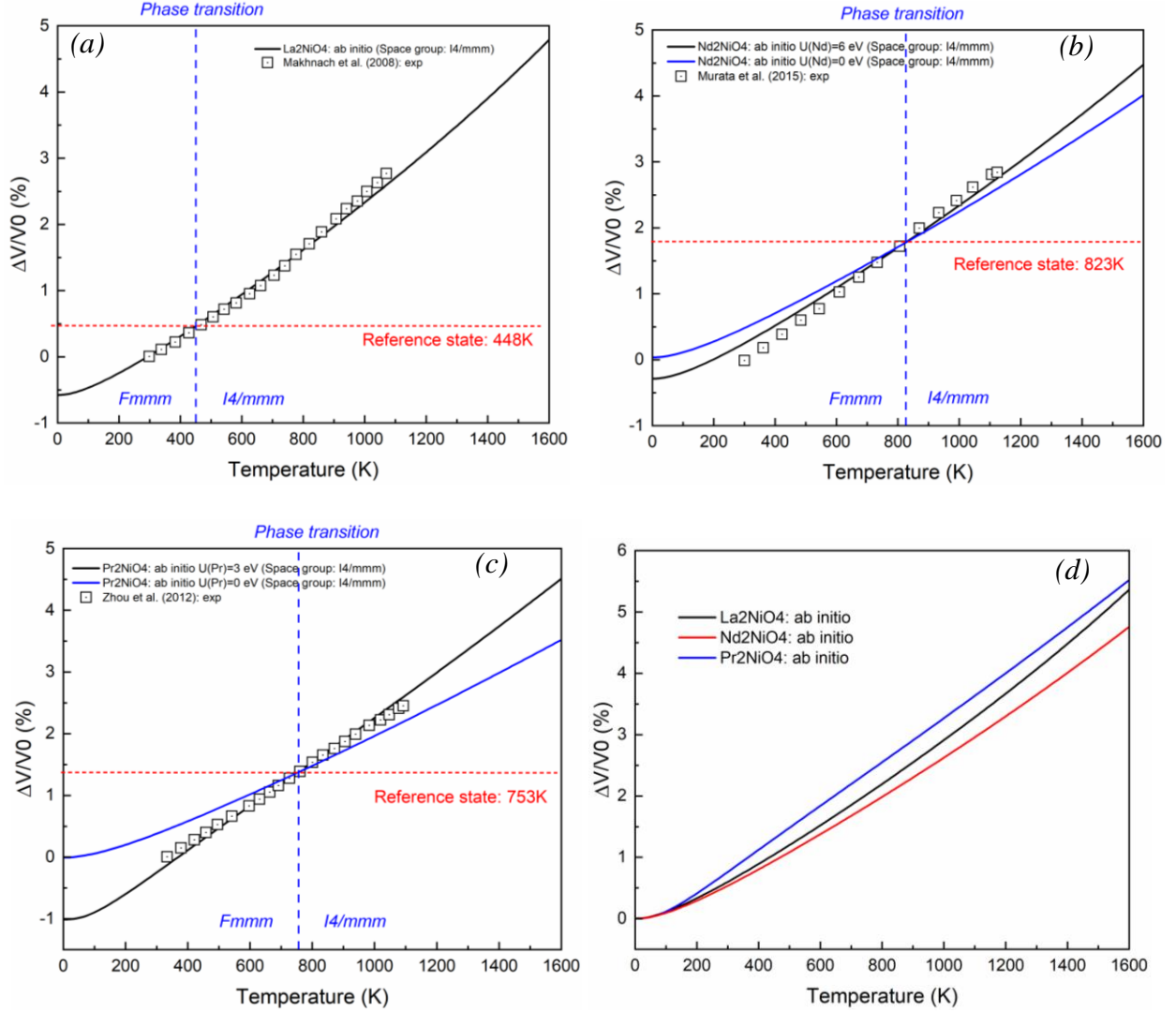


Figure 5 The volume thermal expansion calculated through the combined DFT-QHA method compared with the experimental data [20, 62, 63], (a) La_2NiO_4 , (b) Nd_2NiO_4 , (c) Pr_2NiO_4 , and (d) Comparison using the *ab initio* results.

3.3.2. Extrapolation of temperature-dependent properties of the $\text{Ln}_2\text{NiO}_{4+\delta}$

The temperature-dependent properties of the $\text{Ln}_2\text{NiO}_{4+\delta}$ were derived by applying a systematic three-step procedure. The first step in this procedure is calculating the energy barrier, phonon, and electronic density of states of $\text{Ln}_2\text{NiO}_{4+\delta}$ at 0 K as a function of volumes. In the present study, the calculated volumes are 13.70\AA^3 , 14.11\AA^3 , and 14.53\AA^3 for $\text{La}_2\text{NiO}_{4+\delta}$, 13.12\AA^3 , 13.52\AA^3 ,

and 13.92\AA^3 for $\text{Nd}_2\text{NiO}_{4+\delta}$, and 13.39\AA^3 , 13.80\AA^3 , and 14.21\AA^3 $\text{Pr}_2\text{NiO}_{4+\delta}$, respectively. In the second step, the equilibrium $V_{eq}(P, T)$ at different temperatures is calculated with QHA. In the third step, the calculated physical properties from the first step at the different volumes were approximated by the combination of QHA and the linear regression model. The above procedure assumes that the temperature-dependent properties of the $\text{Ln}_2\text{NiO}_{4+\delta}$ are solely caused by thermal expansion.

In particular, the present work associated the calculated migration energy barriers with the diffusivity and ionic conductivity with the transition state theory [67] and Nernst-Einstein relation [68] as:

$$D(V, T) = \frac{n_p}{2d} l(V, T)^2 v_0 \exp\left(-\frac{\Delta E_b(V, T)}{k_B T}\right) \quad (9)$$

$$v_0 = \frac{k_B T}{h} \exp\left(-\frac{\Delta F_{vib}(V, T)}{k_B T}\right) \quad (10)$$

$$\sigma(V, T) = \frac{Nq^2 D(V, T)}{V(T)k_B T} \quad (11)$$

where v_0 represents the attempt frequency (**See S6 in the supplementary file**), $\Delta F_{vib}(V, T)$ is the vibrational free energy difference (**See S7 in the supplementary file**) between the transition (saddle-point) state and the equilibrium (binding or stable) state, $l(V, T)$ and $\Delta E_b(V, T)$ denote the hopping distance and energy barrier at different volumes and temperatures, respectively (**See S8 in the supplementary file**). The hopping distance is approximately equal to the migration distance of the NEB process. N is the number of mobile carriers. n_p is the number of equivalent diffusion paths ($n_p=4$ corresponds to the four available directions around the interstitial oxygen for the push-pull interstitialcy mechanism). d is the dimension of the space where the diffusion process occurs

($d=3$ since we compare our results to experimental data primarily for ceramics, in which a - b planes are randomly oriented).

As n_p , d , l , and $V(T)$ are identical or similar in $\text{La}_2\text{NiO}_{4+\delta}$, $\text{Nd}_2\text{NiO}_{4+\delta}$, and $\text{Pr}_2\text{NiO}_{4+\delta}$, the differences in diffusion coefficients and ionic conductivity should arise from activation energy barriers ΔE_b and attempt frequencies ν_0 . The calculated attempt frequencies are shown in *Figure S6 (in the supplementary file)*. As seen in the figure, the attempt frequencies of all these three compounds rise with the increasing temperature. Among all these three compounds, the $\text{Pr}_2\text{NiO}_{4+\delta}$ exhibits much higher attempt frequencies at high temperatures. The resulting frequency reaches 5.2 THz at 1600K. Overall, the calculated attempt frequencies are in the range of the usually assumed value from the literature (1-10 THz) [69, 70].

The predicted temperature-dependent properties of volume, energy barrier, hopping distance, diffusivity, and ionic conductivity are shown in Figure 6. Generally, the volume of solid material increases linearly with the increase in temperatures. To approximate the temperature-dependent properties, the linear regression model was adopted to fit the *ab initio* data calculated by QHA. Particularly, the solid red curve on the first sub-graph represents the predicted temperature-dependent EOS based on QHA, as discussed in the previous section. The black circles represent the *ab-initio* calculation results. The linear regression approach was used to derive the relationship between Volume vs. Temperature, Volume vs. Energy barrier, and Volume vs. Hopping distance (based on the *ab-initio* results) because all these properties are linearly related to temperature. The fitting results are shown as black dashed lines in Figure 6. Eventually, the diffusivity and conductivity with the temperature change were predicted.

Based on Figure 6, it is observed that the fitted linear curves exhibit good agreement with the *ab initio* data, which can reasonably represent the temperature-dependent properties of the

$\text{Ln}_2\text{NiO}_{4+\delta}$. Generally, it is observed that the hopping distance, diffusivity, and ionic conductivity gradually increase with the increasing temperature, whereas the energy barrier decreases steadily with the temperature increase.

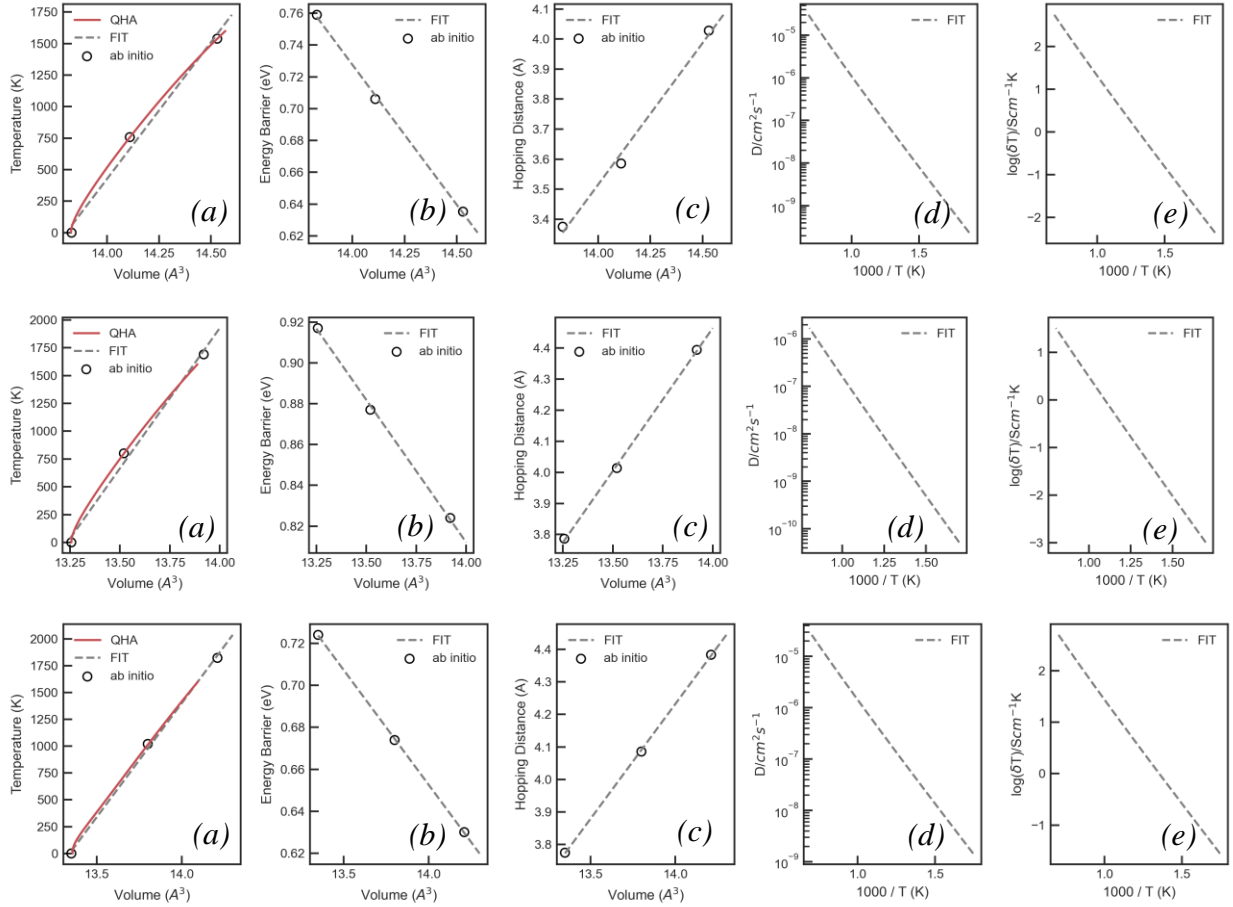


Figure 6 The temperature-dependent properties of $\text{Ln}_2\text{NiO}_{4+\delta}$ (a) Thermal expansion (b) Energy barrier (c) Hopping distance (d) Diffusivity (e) Ionic conductivity (Note: First row: $\text{La}_2\text{NiO}_{4+\delta}$ Second row: $\text{Nd}_2\text{NiO}_{4+\delta}$ Third row: $\text{Pr}_2\text{NiO}_{4+\delta}$)

3.4 The comparison between *ab initio* with experimental data

3.4.1. Diffusion coefficient

The Arrhenius plots of $\text{Ln}_2\text{NiO}_{4+\delta}$ comparing the predicted diffusion coefficient with previous experimental data [22, 23, 71, 72] and modeling data [25] are shown in Figure 7. The green dashed lines represent the diffusion coefficient predicted according to the temperature-dependent energy barrier (see Eq. (8)). In contrast, the solid red lines denote the diffusion coefficient calculated from Eq. (8), using 0 K values for l and ΔE_b , and assuming that these quantities are temperature-independent.

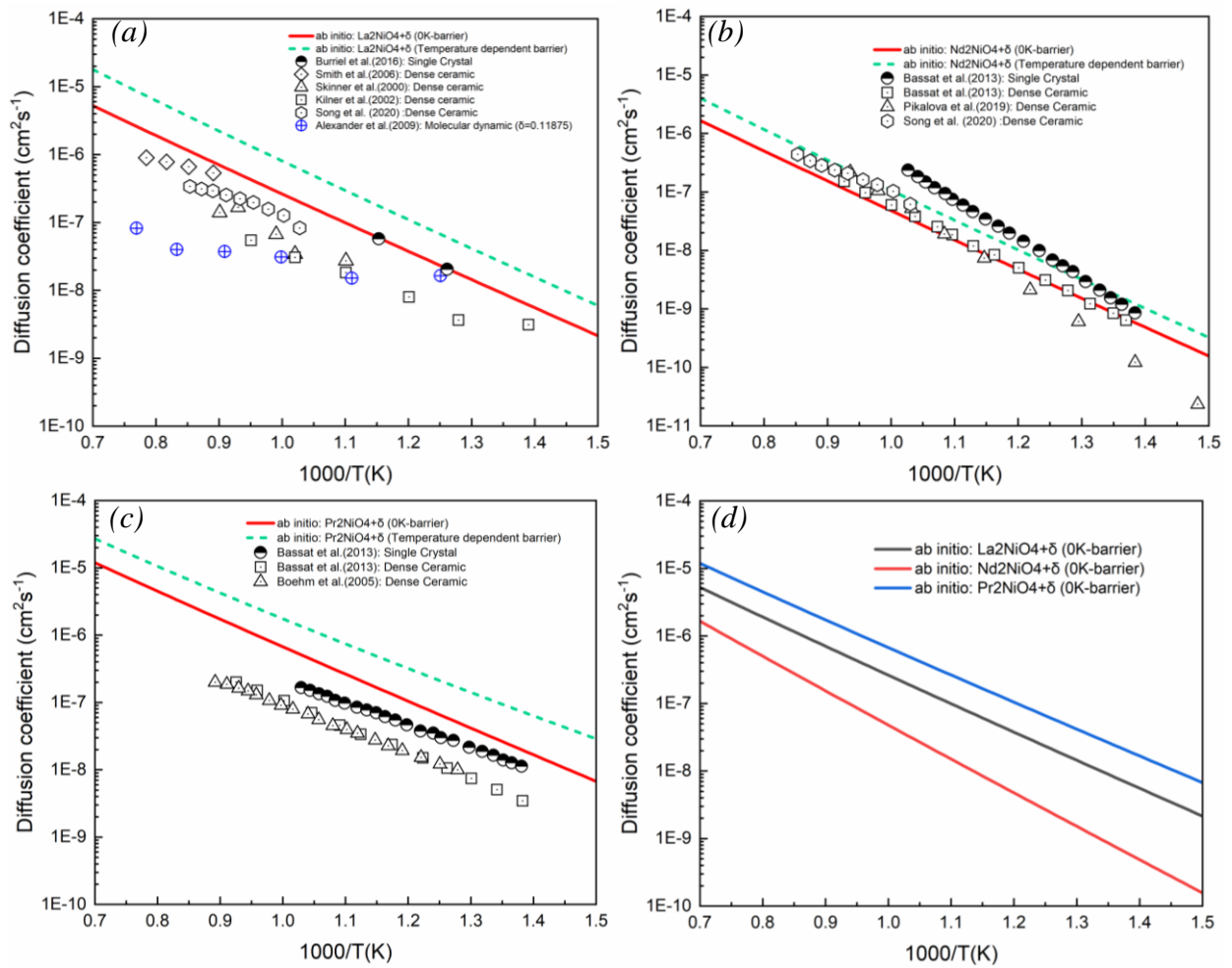


Figure 7 The *ab initio* predicted diffusion coefficient, including the comparison with experimental data [22, 23, 64, 71, 72] and modeling data [25] (a) $\text{La}_2\text{NiO}_{4+\delta}$ (b) $\text{Nd}_2\text{NiO}_{4+\delta}$ (c) $\text{Pr}_2\text{NiO}_{4+\delta}$ (d) Comparison

In the case of $\text{La}_2\text{NiO}_{4+\delta}$, as shown in Figure 7 (a), the estimated activation energy barrier at 0 K (considering the contribution from phonon) is 0.759 eV, which is very close to the experimental activation energy by Skinner et al. [22] ($\Delta E_b=0.85$ eV) for the dense ceramic. Notably, compared with the activation energy barrier ($\Delta E_b=0.51$ eV) predicted by Alexander et al. [25] using the molecular dynamic simulation (blue marks), the current *ab initio* calculation yields a much closer value of activation energy barrier with the experimental data [22, 71]. For the results of $\text{Nd}_2\text{NiO}_{4+\delta}$ and $\text{Pr}_2\text{NiO}_{4+\delta}$ (Figure 7 (b) and (c)), the *ab initio* calculated activation energies at 0 K are 0.917 eV and 0.724 eV, respectively, which are similar to the experimental values [23] for the dense ceramic $\text{Nd}_2\text{NiO}_{4+\delta}$ ($\Delta E_b=1.1$ eV) and $\text{Pr}_2\text{NiO}_{4+\delta}$ ($\Delta E_b=0.8$ eV). However, while the slope of the diffusion coefficient was successfully reproduced, the estimated pre-exponential factors of $\text{La}_2\text{NiO}_{4+\delta}$ and $\text{Pr}_2\text{NiO}_{4+\delta}$ by the transition state theory are slightly higher than the experimental data. The reason for this discrepancy will be discussed in *Section 3.4.3*. In addition, Figure 7 (d) compares the diffusion coefficients in these three over-stoichiometric compounds. According to our prediction, it can be observed that the ionic diffusivities of the $\text{Ln}_2\text{NiO}_{4+\delta}$ rank as $\text{Pr}_2\text{NiO}_{4+\delta} > \text{La}_2\text{NiO}_{4+\delta} > \text{Nd}_2\text{NiO}_{4+\delta}$.

Overall, our *ab initio* predicted diffusion coefficients have a reasonable agreement with experimental data of $\text{La}_2\text{NiO}_{4+\delta}$, $\text{Nd}_2\text{NiO}_{4+\delta}$, and $\text{Pr}_2\text{NiO}_{4+\delta}$, especially for the single crystal data [23, 72]. It is because the single crystal has infinite periodicity in which the crystal lattice of the entire sample is continuous with no grain boundaries, defects, and domain walls, which is closer to the *ab initio* calculated structure. Meanwhile, it was found that the predicted diffusion

coefficients based on the 0 K barriers have much better consistency with the experimental data than the results from the temperature-dependent barrier. While the results based on the 0 K barrier yield better agreement with the experimental data, the present work believes that the properties predicted according to the temperature-dependent barrier have more physical meaning because of considering the temperature effect.

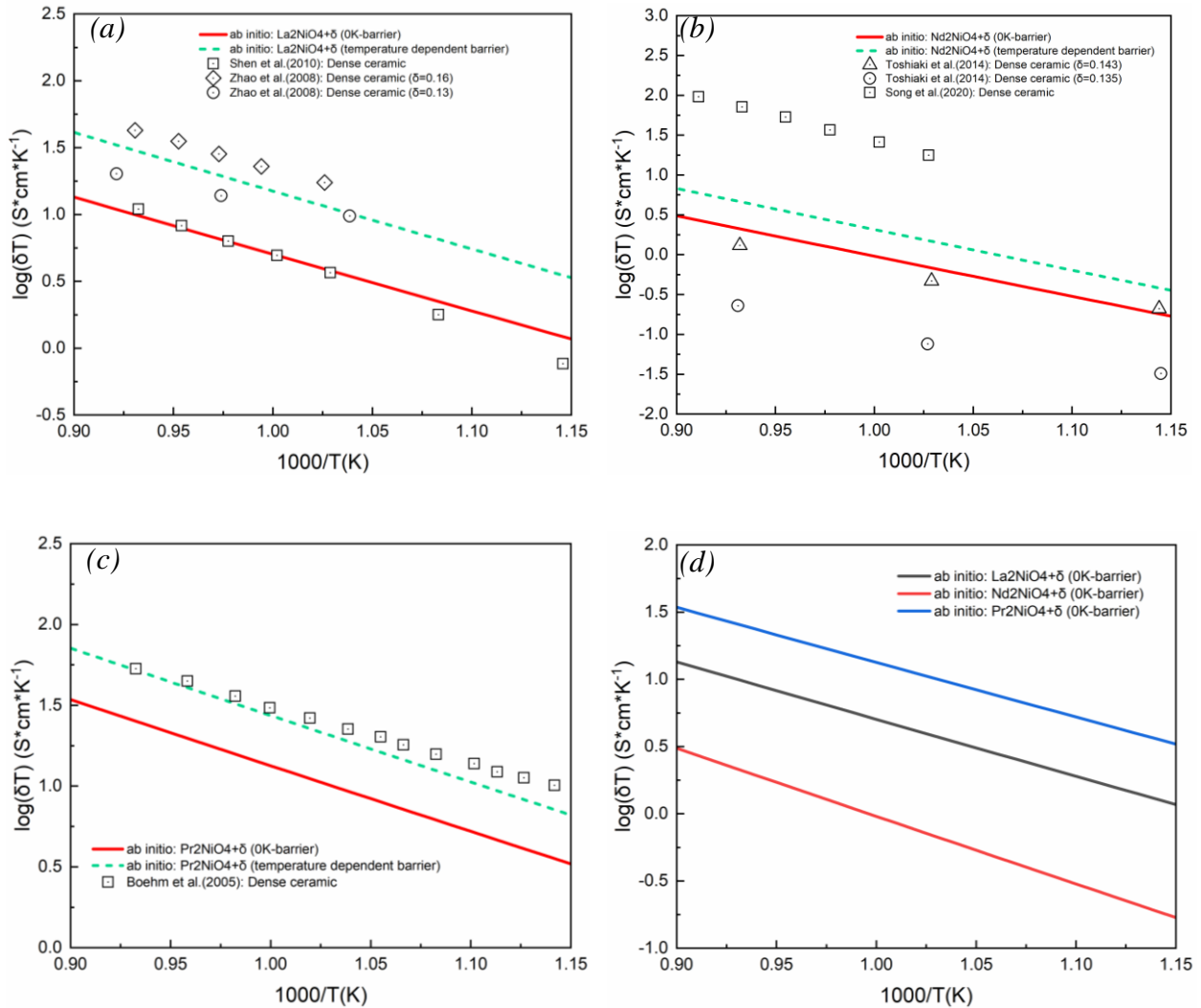


Figure 8 The *ab initio* predicted ionic conductivity, including the comparison with experimental data [9, 24, 64, 73, 74] (a) $La_2NiO_{4+\delta}$ (b) $Nd_2NiO_{4+\delta}$ (c) $Pr_2NiO_{4+\delta}$ (d) Comparison.

3.4.2. Ionic conductivity

The Arrhenius plots for ionic conductivity of $\text{Ln}_2\text{NiO}_{4+\delta}$ as a function of temperatures are shown in Figure 8. The comparisons between the *ab initio* and experimental data [9, 24, 64, 73, 74] are also included in the figure. Similarly, the solid red and green dash lines denote the ionic conductivities predicted by the 0 K and temperature-dependent barriers, respectively. It is shown that, according to Figure 8, the predicted ionic conductivity increases linearly with the increasing temperature, which reasonably agrees well with the experimental data [9, 24, 64, 73, 74], except for the $\text{Nd}_2\text{NiO}_{4+\delta}$. However, it is hard to conclude the reliability of our prediction on $\text{Nd}_2\text{NiO}_{4+\delta}$ because the experimental data measured by the different groups have huge fluctuation. Generally, the ionic conductivity is proportional to the diffusion coefficient, which typically scales with the value of the activation energy barrier. It has been reported that the activation energy barrier of $\text{Nd}_2\text{NiO}_{4+\delta}$ ($\Delta E_b=1.1$ eV [23]) is much higher than $\text{La}_2\text{NiO}_{4+\delta}$ ($\Delta E_b=0.85\sim 0.88$ eV [22]) and $\text{Pr}_2\text{NiO}_{4+\delta}$ ($\Delta E_b=0.8$ eV [23]). Therefore, it can be speculated that the ionic conductivity value for $\text{Nd}_2\text{NiO}_{4+\delta}$ should be lower than that of $\text{La}_2\text{NiO}_{4+\delta}$ and $\text{Pr}_2\text{NiO}_{4+\delta}$. Accordingly, it is suggested that more experimental work should be carried out to investigate the ionic conductivity of $\text{Nd}_2\text{NiO}_{4+\delta}$. Finally, our *ab initio* predictions show that the $\text{Pr}_2\text{NiO}_{4+\delta}$ exhibits the highest ionic conductivity (see Figure 8 (d)) among all these three over-stoichiometric compounds due to the lowest activation energy barrier.

3.4.3. Discussion on the discrepancies between *ab initio* calculations and experimental data

Even though the consistency between our *ab initio* prediction and experimental value in $\text{Ln}_2\text{NiO}_{4+\delta}$ compounds is generally acceptable, there are still some discrepancies, such as the pre-

exponential factors. In this section, several reasons for the discrepancies between the *ab initio* prediction and experimental data are listed:

- i. The oxygen hyper-stoichiometry δ in $\text{Ln}_2\text{NiO}_{4+\delta}$ compounds will change with the temperature and oxygen partial pressure, which was not considered in the present study. Therefore, any changes in δ will directly affect the carrier concentration and, in turn, the conductivities.
- ii. The reliability of the PBE exchange-correlation functional on predicting transition metal oxides and rare-earth compounds is still in question. While the GGA+ U approach is able to make some corrections, it is yet to make an accurate prediction.
- iii. The size of the supercell and the number of images adopted for the NEB calculations may also affect the prediction reliabilities.
- iv. The temperature-dependent properties are assumed to be only attributed to the thermal expansion coefficient. However, there may be other factors having an impact on the properties.
- v. The discrepancies may also come from the influence of defects in real materials (grain boundaries, domain walls, non-homogeneities, etc.), which could somewhat hinder the diffusivity and ionic conductivity.
- vi. The observed diffusion coefficient of dense ceramics is a weighted average of the diffusion coefficients along the a - b plane and c direction. However, the diffusion coefficient along the c direction was neglected in the present work due to its high energy barrier.

Overall, the activation energy barriers are reasonably reproduced by the *ab initio* calculations. Meanwhile, the ranking between the $\text{La}_2\text{NiO}_{4+\delta}$, $\text{Nd}_2\text{NiO}_{4+\delta}$, and $\text{Pr}_2\text{NiO}_{4+\delta}$ for both the activation energy barrier and diffusion coefficient is in good agreement with the experimental data. However,

the calculated value for pre-exponential factors is far more speculative due to the inherently approximate methods for predicting attempt frequency values *in silico* (1THz~10THz).

4. Conclusion

In the present work, the vacancy formation energy, diffusivity, and ionic conductivity of the $Ln_2NiO_{4+\delta}$ ($\delta=0.125$) RP phase was systematically investigated through the *ab initio* approach. Firstly, the NEB method is adopted to predict the oxygen ions' energy barrier, which is then utilized to derive the diffusion coefficient and ionic conductivity using the transition state theory and the Nernst-Einstein relation. Secondly, a combination of QHA and a linear regression model is used to study and reproduce the temperature-dependent properties of the $Ln_2NiO_{4+\delta}$ materials. As a result, in agreement with previous theoretical and experimental works in literature, the following conclusions can be reached:

- i. The vacancy diffusion does not play a dominant role in the Ln_2NiO_4 phase due to the high vacancy formation energy.
- ii. The interstitial O^{2-} of the $Ln_2NiO_{4+\delta}$ phase should migrate parallel to the *a-b* plane (interstitialcy mechanism) instead of the *c* direction.
- iii. Among all the three compounds, the $Pr_2NiO_{4+\delta}$ exhibits the lowest activation energy barrier and highest thermal expansion, diffusivity, and ionic conductivity.

The predicted energy barrier, diffusion coefficient, and ionic conductivity of $Ln_2NiO_{4+\delta}$ exhibit reasonable agreement with the experimental data. Meanwhile, the computational method developed in this study is an easy, time-efficient, and reliable tool for accessing oxygen diffusivity properties as a function of temperature in oxide material, in which the temperature dependence is predominantly caused by thermal expansion.

The fixed oxygen hyper-stoichiometries, DFT exchange-correlation functional, supercell size, defects, etc., might cause the discrepancies observed for the pre-exponential factors. Therefore, more accurate methods to calculate the attempt frequencies are needed to improve the agreement between the *ab initio* and the experimental results.

5. Acknowledgement

This material is based upon work supported by the Department of Energy under Award Number DE-FE0031972 and Advanced Cyberinfrastructure Coordination Ecosystem: Services & Support (ACCESS) program Award Numbers TG-DMR190004. In addition, the authors would like to thank the technical support from the Academic & Research Computing team at Worcester Polytechnic Institute, especially James Leonard Kingsley and Siamak Mohammed Z. Najafi.

References

- [1] M. Mogensen, M. Chen, H. Frandsen, C. Graves, J. Hansen, K. Hansen, A. Hauch, T. Jacobsen, S. Jensen, T. Skaftø, Reversible solid-oxide cells for clean and sustainable energy, *Clean Energy*, 3 (2019) 175-201.
- [2] M.-B. Choi, B. Singh, E.D. Wachsman, S.-J. Song, Performance of $\text{La}_{0.1}\text{Sr}_{0.9}\text{Co}_{0.8}\text{Fe}_{0.2}\text{O}_{3-\delta}$ and $\text{La}_{0.1}\text{Sr}_{0.9}\text{Co}_{0.8}\text{Fe}_{0.2}\text{O}_{3-\delta}\text{-Ce}_{0.9}\text{Gd}_{0.1}\text{O}_2$ oxygen electrodes with $\text{Ce}_{0.9}\text{Gd}_{0.1}\text{O}_2$ barrier layer in reversible solid oxide fuel cells, *Journal of Power Sources*, 239 (2013) 361-373.
- [3] Y.-S. Yoo, M. Choi, J.-H. Hwang, H.-N. Im, B. Singh, S.-J. Song, $\text{La}_2\text{NiO}_{4+\delta}$ as oxygen electrode in reversible solid oxide cells, *Ceramics International*, 41 (2015) 6448-6454.
- [4] V. Vibhu, A. Flura, A. Rougier, C. Nicollet, S. Fourcade, T. Hungria, J.-C. Grenier, J.-M. Bassat, Electrochemical ageing study of mixed lanthanum/praseodymium nickelates $\text{La}_{2-x}\text{Pr}_x\text{NiO}_{4+\delta}$ as oxygen electrodes for solid oxide fuel or electrolysis cells, *Journal of Energy Chemistry*, 46 (2020) 62-70.
- [5] H. Jiang, Z. Lu, B. Qian, S. Wang, B. Yin, Y. Zheng, L. Ge, H. Chen, C. Zhang, Bi-doped $\text{La}_{1.5}\text{Sr}_{0.5}\text{Ni}_{0.5}\text{Mn}_{0.5}\text{O}_{4+\delta}$ as an efficient air electrode material for SOEC, *International Journal of Hydrogen Energy*, 46 (2021) 36037-36045.
- [6] M. Ghamarinia, A. Babaei, C. Zamani, Electrochemical characterization of La_2NiO_4 -infiltrated $\text{La}_{0.6}\text{Sr}_{0.4}\text{Co}_{0.2}\text{Fe}_{0.8}\text{O}_{3-\delta}$ by analysis of distribution of relaxation times, *Electrochimica Acta*, 353 (2020) 136520.
- [7] A. Egger, N. Schrödl, C. Gspan, W. Sitte, $\text{La}_2\text{NiO}_{4+\delta}$ as electrode material for solid oxide fuel cells and electrolyzer cells, *Solid State Ionics*, 299 (2017) 18-25.
- [8] J. Hyodo, K. Tominaga, Y.-W. Ju, S. Ida, T. Ishihara, Electrical conductivity and oxygen diffusivity in Cu- and Ga-doped Pr_2NiO_4 , *Solid State Ionics*, 256 (2014) 5-10.
- [9] E. Boehm, J.-M. Bassat, P. Dordor, F. Mauvy, J.-C. Grenier, P. Stevens, Oxygen diffusion and transport properties in non-stoichiometric $\text{Ln}_{2-x}\text{NiO}_{4+\delta}$ oxides, *Solid State Ionics*, 176 (2005) 2717-2725.
- [10] S. Miyoshi, T. Furuno, O. Sangoanruang, H. Matsumoto, T. Ishihara, Mixed conductivity and oxygen permeability of doped Pr_2NiO_4 -based oxides, *Journal of the Electrochemical Society*, 154 (2006) B57.
- [11] A. Shaula, E. Naumovich, A. Viskup, V. Pankov, A. Kovalevsky, V. Kharton, Oxygen transport in $\text{La}_2\text{NiO}_{4+\delta}$: Assessment of surface limitations and multilayer membrane architectures, *Solid State Ionics*, 180 (2009) 812-816.
- [12] Z. Li, R. Haugrud, Effects of surface coatings on the determination of D_{chem} and k_{chem} in $\text{La}_2\text{NiO}_{4+\delta}$ by conductivity relaxation, *Solid State Ionics*, 206 (2012) 67-71.
- [13] N. Čebašek, R. Haugrud, T. Norby, Determination of inter-diffusion coefficients for the A-and B-site in the $\text{A}_2\text{BO}_{4+\delta}$ (A= La, Nd and B= Ni, Cu) system, *Solid State Ionics*, 231 (2013) 74-80.
- [14] A. Egger, W. Sitte, Enhanced oxygen surface exchange of $\text{La}_2\text{NiO}_{4+\delta}$ by means of a thin surface layer of silver, *Solid State Ionics*, 258 (2014) 30-37.
- [15] A. Staykov, T. Nguyen, T. Akbay, T. Ishihara, Oxygen Reduction Reaction and Electronic Properties of LnO-Terminated Surfaces of Pr_2NiO_4 and La_2NiO_4 , *The Journal of Physical Chemistry C*, 126 (2022) 7390-7399.
- [16] M. Burriel, G. Garcia, J. Santiso, J.A. Kilner, R.J. Chater, S.J. Skinner, Anisotropic oxygen diffusion properties in epitaxial thin films of $\text{La}_2\text{NiO}_{4+\delta}$, *Journal of materials chemistry*, 18 (2008) 416-422.
- [17] X. Ma, B. Wang, E. Xhafa, K. Sun, E. Nikolla, Synthesis of shape-controlled $\text{La}_2\text{NiO}_{4+\delta}$ nanostructures and their anisotropic properties for oxygen diffusion, *Chemical Communications*, 51 (2015) 137-140.
- [18] M. Ananyev, E. Tropin, V. Eremin, A. Farlenkov, A. Smirnov, A. Kolchugin, N. Porotnikova, A. Khodimchuk, A. Berenov, E.K. Kurumchin, Oxygen isotope exchange in $\text{La}_2\text{NiO}_{4\pm\delta}$, *Physical Chemistry Chemical Physics*, 18 (2016) 9102-9111.
- [19] N. Han, Z. Shen, X. Zhao, R. Chen, V.K. Thakur, Perovskite oxides for oxygen transport: Chemistry and material horizons, *Science of The Total Environment*, 806 (2022) 151213.

- [20] A. Murata, T. Uchikoshi, M. Matsuda, Fabrication and characterization of oriented Nd₂NiO₄ bulk and cathode for low-temperature operating solid oxide fuel cell, *Journal of Power Sources*, 293 (2015) 95-100.
- [21] C. Munnings, S. Skinner, G. Amow, P. Whitfield, I. Davidson, Oxygen transport in the La₂Ni_{1-x}CoxO_{4+δ} system, *Solid State Ionics*, 176 (2005) 1895-1901.
- [22] S. Skinner, J. Kilner, Oxygen diffusion and surface exchange in La_{2-x}SrxNiO_{4+δ}, *Solid State Ionics*, 135 (2000) 709-712.
- [23] J.-M. Bassat, M. Burriel, O. Wahyudi, R.m. Castaing, M. Ceretti, P. Veber, I. Weill, A. Villesuzanne, J.-C. Grenier, W. Paulus, Anisotropic oxygen diffusion properties in Pr₂NiO_{4+δ} and Nd₂NiO_{4+δ} single crystals, *The Journal of Physical Chemistry C*, 117 (2013) 26466-26472.
- [24] Y. Shen, H. Zhao, X. Liu, N. Xu, Preparation and electrical properties of Ca-doped La₂NiO_{4+δ} cathode materials for IT-SOFC, *Physical chemistry chemical physics*, 12 (2010) 15124-15131.
- [25] A. Chroneos, D. Parfitt, J.A. Kilner, R.W. Grimes, Anisotropic oxygen diffusion in tetragonal La₂NiO_{4+δ}: molecular dynamics calculations, *Journal of Materials Chemistry*, 20 (2010) 266-270.
- [26] D. Parfitt, A. Chroneos, J.A. Kilner, R.W. Grimes, Molecular dynamics study of oxygen diffusion in Pr₂NiO_{4+δ}, *Physical Chemistry Chemical Physics*, 12 (2010) 6834-6836.
- [27] A. Perrichon, A. Piovano, M. Boehm, M. Zbiri, M. Johnson, H. Schober, M. Ceretti, W. Paulus, Lattice dynamics modified by excess oxygen in Nd₂NiO_{4+δ}: triggering low-temperature oxygen diffusion, *The Journal of Physical Chemistry C*, 119 (2015) 1557-1564.
- [28] S. Xu, R. Jacobs, D. Morgan, Factors Controlling Oxygen Interstitial Diffusion in the Ruddlesden–Popper Oxide La_{2-x}SrxNiO_{4+δ}, *Chemistry of Materials*, 30 (2018) 7166-7177.
- [29] C. Frayret, A. Villesuzanne, M. Pouchard, Application of density functional theory to the modeling of the mixed ionic and electronic conductor La₂NiO_{4+δ}: Lattice relaxation, oxygen mobility, and energetics of frenkel defects, *Chemistry of materials*, 17 (2005) 6538-6544.
- [30] L. Minervini, R.W. Grimes, J.A. Kilner, K.E. Sickafus, Oxygen migration in La₂NiO_{4+δ}, *Journal of Materials Chemistry*, 10 (2000) 2349-2354.
- [31] A. Villesuzanne, W. Paulus, A. Cousson, S. Hosoya, L. Le Dréau, O. Hernandez, C. Prestipino, M. Ikbél Houchati, J. Schefer, On the role of lattice dynamics on low-temperature oxygen mobility in solid oxides: a neutron diffraction and first-principles investigation of, *Journal of Solid State Electrochemistry*, 15 (2011) 357-366.
- [32] L. Zhang, F. Yao, J. Meng, W. Zhang, H. Wang, X. Liu, J. Meng, H. Zhang, Oxygen migration and proton diffusivity in transition-metal (Mn, Fe, Co, and Cu) doped Ruddlesden–Popper oxides, *Journal of Materials Chemistry A*, 7 (2019) 18558-18567.
- [33] N.A. Szaro, S.C. Ammal, F. Chen, A. Heyden, An ab initio study of the oxygen defect formation and oxide ion migration in (Sr_{1-x}Pr_x)₂FeO_{4±δ}, *Journal of Power Sources*, 515 (2021) 230602.
- [34] X. Li, N.A. Benedek, Enhancement of ionic transport in complex oxides through soft lattice modes and epitaxial strain, *Chemistry of Materials*, 27 (2015) 2647-2652.
- [35] W. Xie, Y.-L. Lee, Y. Shao-Horn, D. Morgan, Oxygen Point Defect Chemistry in Ruddlesden–Popper Oxides (La_{1-x}Srx)₂MO_{4±δ} (M= Co, Ni, Cu), *The journal of physical chemistry letters*, 7 (2016) 1939-1944.
- [36] A. Flura, J. Laurencin, S. Fourcade, F. Mauvy, V. Vibhu, J.-P. Salvétat, J. Mouginn, J.-M. Bassat, Development of an Isotopic Oxygen Exchange Setup Operating Under High Pressure: Preliminary Measurements Performed on Ln₂NiO_{4+δ} (Ln= La, Pr, Nd, MIEC) Oxides, *ECS Transactions*, 103 (2021) 1319.
- [37] V.A. Sadykov, E. Pikalova, A.A. Kolchugin, N.F. Ereemeev, N.M. Bogdanovich, A.F. Khasanov, P.I. SKRIABIN, A.V. KRASNOV, E. Sadovskaya, A. Shmakov, Transport properties of Ca-doped Ln₂NiO₄, 10TH International Conference on Sustainable Energy and Environmental Protection Hydrogen and Fuel Cells, 2017, pp. 87.
- [38] G.K. Madsen, A. Katre, C. Bera, Calculating the thermal conductivity of the silicon clathrates using the quasi - harmonic approximation, *physica status solidi (a)*, 213 (2016) 802-807.

- [39] Y. Wang, J. Wang, H. Zhang, V. Manga, S. Shang, L. Chen, Z. Liu, A first-principles approach to finite temperature elastic constants, *Journal of Physics: Condensed Matter*, 22 (2010) 225404.
- [40] D. Ma, B. Grabowski, F. Körmann, J. Neugebauer, D. Raabe, Ab initio thermodynamics of the CoCrFeMnNi high entropy alloy: Importance of entropy contributions beyond the configurational one, *Acta Materialia*, 100 (2015) 90-97.
- [41] G. Kresse, J. Furthmüller, Efficient iterative schemes for ab initio total-energy calculations using a plane-wave basis set, *Physical review B*, 54 (1996) 11169.
- [42] G. Kresse, J. Furthmüller, Efficiency of ab-initio total energy calculations for metals and semiconductors using a plane-wave basis set, *Computational materials science*, 6 (1996) 15-50.
- [43] J.P. Perdew, J.A. Chevary, S.H. Vosko, K.A. Jackson, M.R. Pederson, D.J. Singh, C. Fiolhais, Atoms, molecules, solids, and surfaces: Applications of the generalized gradient approximation for exchange and correlation, *Physical review B*, 46 (1992) 6671.
- [44] J.P. Perdew, K. Burke, M. Ernzerhof, Generalized gradient approximation made simple, *Physical review letters*, 77 (1996) 3865.
- [45] P.E. Blöchl, O. Jepsen, O.K. Andersen, Improved tetrahedron method for Brillouin-zone integrations, *Physical Review B*, 49 (1994) 16223.
- [46] F.D. Murnaghan, Finite deformations of an elastic solid, *American Journal of Mathematics*, 59 (1937) 235-260.
- [47] Y.-L. Lee, J. Kleis, J. Rossmeisl, D. Morgan, Ab initio energetics of La B O 3 (001)(B= Mn, Fe, Co, and Ni) for solid oxide fuel cell cathodes, *Physical Review B*, 80 (2009) 224101.
- [48] V.I. Anisimov, F. Aryasetiawan, A. Lichtenstein, First-principles calculations of the electronic structure and spectra of strongly correlated systems: the LDA+ U method, *Journal of Physics: Condensed Matter*, 9 (1997) 767.
- [49] G. Pacchioni, Modeling doped and defective oxides in catalysis with density functional theory methods: Room for improvements, *The Journal of chemical physics*, 128 (2008) 182505.
- [50] T. Akbay, A. Staykov, J. Druce, H. Téllez, T. Ishihara, J.A. Kilner, The interaction of molecular oxygen on LaO terminated surfaces of La₂NiO₄, *Journal of Materials Chemistry A*, 4 (2016) 13113-13124.
- [51] Y. Wang, L.-Q. Chen, Z.-K. Liu, YPHON: A package for calculating phonons of polar materials, *Computer Physics Communications*, 185 (2014) 2950-2968.
- [52] G. Henkelman, B.P. Uberuaga, H. Jónsson, A climbing image nudged elastic band method for finding saddle points and minimum energy paths, *The Journal of chemical physics*, 113 (2000) 9901-9904.
- [53] K. Momma, F. Izumi, VESTA 3 for three-dimensional visualization of crystal, volumetric and morphology data, *Journal of applied crystallography*, 44 (2011) 1272-1276.
- [54] Z.-G. Mei, S.-L. Shang, Y. Wang, Z.-K. Liu, Density-functional study of the thermodynamic properties and the pressure–temperature phase diagram of Ti, *Physical Review B*, 80 (2009).
- [55] Y. Wang, Z.K. Liu, L.Q. Chen, Thermodynamic properties of Al, Ni, NiAl, and Ni₃Al from first-principles calculations, *Acta Materialia*, 52 (2004) 2665-2671.
- [56] Y. Wang, R. Ahuja, B. Johansson, Mean - field potential approach to the quasiharmonic theory of solids, *International journal of quantum chemistry*, 96 (2004) 501-506.
- [57] F. Körmann, A. Dick, B. Grabowski, B. Hallstedt, T. Hickel, J. Neugebauer, Free energy of bcc iron: Integrated ab initio derivation of vibrational, electronic, and magnetic contributions, *Physical Review B*, 78 (2008).
- [58] A. Cleave, J. Kilner, S. Skinner, S. Murphy, R. Grimes, Atomistic computer simulation of oxygen ion conduction mechanisms in La₂NiO₄, *Solid State Ionics*, 179 (2008) 823-826.
- [59] J. Jorgensen, B. Dabrowski, S. Pei, D. Richards, D. Hinks, Structure of the interstitial oxygen defect in La₂NiO_{4+δ}, *Physical Review B*, 40 (1989) 2187.
- [60] E. Magnone, G. Cerisola, M. Ferretti, A. Barbucci, Electrochemical Investigation of Oxygen Intercalation into La₂CuO_{4+δ} Phases, *Journal of Solid State Chemistry*, 144 (1999) 8-15.

- [61] J.C. Grenier, F. Mauvy, C. Lalanne, J.-M. Bassat, F. Chauveau, J. Mougín, J. Dailly, M. Marrony, $A_2MO_{4+\delta}$ oxides: flexible electrode materials for solid oxide cells, *ECS Transactions*, 25 (2009) 2537.
- [62] L.V. Makhnach, V.V. Pankov, P. Strobel, High-temperature oxygen non-stoichiometry, conductivity and structure in strontium-rich nickelates $La_{2-x}Sr_xNiO_{4-\delta}$ ($x = 1$ and 1.4), *Materials Chemistry and Physics*, 111 (2008) 125-130.
- [63] X.-D. Zhou, J.W. Templeton, Z. Nie, H. Chen, J.W. Stevenson, L.R. Pederson, Electrochemical performance and stability of the cathode for solid oxide fuel cells: V. high performance and stable Pr_2NiO_4 as the cathode for solid oxide fuel cells, *Electrochimica Acta*, 71 (2012) 44-49.
- [64] J. Song, D. Ning, B. Boukamp, J.-M. Bassat, H.J. Bouwmeester, Structure, electrical conductivity and oxygen transport properties of Ruddlesden–Popper phases $Ln_{n+1}Ni_nO_{3n+1}$ ($Ln = La, Pr$ and Nd ; $n = 1, 2$ and 3), *Journal of Materials Chemistry A*, 8 (2020) 22206-22221.
- [65] T. Broux, C. Prestipino, M. Bahout, S. Paofai, E. Elkaim, V. Vibhu, J.-C. Grenier, A. Rougier, J.-M. Bassat, O. Hernandez, Structure and reactivity with oxygen of $Pr_2NiO_{4+\delta}$: an in situ synchrotron X-ray powder diffraction study, *Dalton Transactions*, 45 (2016) 3024-3033.
- [66] J. Carvill, *Mechanical engineer's data handbook*, Butterworth-Heinemann, 1994.
- [67] L. Kong, L.J. Lewis, Transition state theory of the preexponential factors for self-diffusion on Cu, Ag, and Ni surfaces, *Physical Review B*, 74 (2006) 073412.
- [68] Y. Liu, S. Wang, A.M. Nolan, C. Ling, Y. Mo, Tailoring the Cation Lattice for Chloride Lithium - Ion Conductors, *Advanced Energy Materials*, 10 (2020) 2002356.
- [69] J. Koettgen, T. Zacherle, S. Grieshammer, M. Martin, Ab initio calculation of the attempt frequency of oxygen diffusion in pure and samarium doped ceria, *Physical Chemistry Chemical Physics*, 19 (2017) 9957-9973.
- [70] J. Koettgen, M. Martin, The Effect of Jump Attempt Frequencies on the Ionic Conductivity of Doped Ceria, *The Journal of Physical Chemistry C*, 123 (2019) 19437-19446.
- [71] J. Kilner, C. Shaw, Mass transport in $La_2Ni_{1-x}Co_xO_{4+\delta}$ oxides with the K_2NiF_4 structure, *Solid State Ionics*, 154 (2002) 523-527.
- [72] M.n. Burriel, H. Téllez, R.J. Chater, R. Castaing, P. Veber, M. Zaghrioui, T. Ishihara, J.A. Kilner, J.-M. Bassat, Influence of crystal orientation and annealing on the oxygen diffusion and surface exchange of $La_2NiO_{4+\delta}$, *The Journal of Physical Chemistry C*, 120 (2016) 17927-17938.
- [73] T. Ina, Y. Orikasa, T. Masese, T. Nakao, A. Mineshige, K. Amezawa, H. Tanida, T. Uruga, Y. Uchimoto, Relationship between Local Structure and Oxide Ionic Diffusion of $Nd_2NiO_{4+\delta}$ with K_2NiF_4 Structure, *Electrochemistry*, 82 (2014) 875-879.
- [74] H. Zhao, F. Mauvy, C. Lalanne, J.-M. Bassat, S. Fourcade, J.-C. Grenier, New cathode materials for ITSOFC: phase stability, oxygen exchange and cathode properties of $La_{2-x}NiO_{4+\delta}$, *Solid State Ionics*, 179 (2008) 2000-2005.